Photobleaching and photoenhancement of endogenous fluorescence observed in two-photon microscopy with broadband laser sources

2010 J. Opt. 12 084006

(http://iopscience.iop.org/2040-8986/12/8/084006)

IOP Publishing Journal of Optics
J. Opt. **12** (2010) 084006 (8pp) doi:10.1088/2040-8978/12/8/084006

Photobleaching and photoenhancement of endogenous fluorescence observed in two-photon microscopy with broadband laser sources

D Pestov, Y Andegeko, V V Lozovoy and M Dantus

Department of Chemistry, Michigan State University, East Lansing, MI 48824, USA

E-mail: dantus@msu.edu

Received 18 February 2010, accepted for publication 4 June 2010
Published 15 July 2010
Online at stacks.iop.org/JOpt/12/084006

Abstract
We examine the effects of pulse duration tuning on the photodamage inflicted by laser light illumination on the imaged sample and, thereby, explore the optimization of optical pulse parameters for multiphoton microscopy imaging under variable conditions. We discuss the dependence of the nonlinear excitation efficiency and associated photodamage rates on pulse energy and duration, and use the controlled amount of second-order dispersion (linear chirp), introduced by a pulse shaper, to adjust the pulse duration at the imaging plane of the microscope. The pulse energy is varied to maintain a constant two-photon excitation efficiency when switching between short (∼14 fs) and long (∼280 fs) pulses, and the damage is assessed by monitoring the photobleaching rates and sample morphology. We have found that in addition to the well-known photobleaching effects, significant enhancement of the two-photon excited autofluorescence intensity can be observed. Photobleaching rates at the onset of the laser light exposure are shown to be independent of the pulse shape under our experimental conditions, which indicates that the primary damage (bleaching) mechanism stems from the two-photon excitation process. The photoenhancement, however, is found to occur more readily with longer pulses, having higher energies per pulse. Experiments are carried out on human melanoma tissue and on rabbit red blood cells.

Keywords: ultrafast, multiphoton, imaging, laser-induced damage, photobleaching, photosensitization

(Some figures in this article are in colour only in the electronic version)

1. Introduction

Since the introduction of multiphoton microscopy (MPM) in the pioneering work by Denk and Webb [1], phototoxicity of the laser radiation, especially if the imaging is done *in vivo*, has been an outstanding concern of imaging-dependent disciplines. Obviously, laser-safe imaging considerations put an upper bound on both laser pulse energy and its peak intensity. The first is related to linear damage mechanisms such as linear absorption and heating of the sample. The second is associated with nonlinear (NL) damage mechanisms. For a conventional two-photon microscope with a 100–200 fs laser source, it is now widely accepted that the major contributors towards phototoxicity in cells [2–4] are two-to-three photon absorption processes that, e.g., trigger formation of reactive oxygen radicals [3], induce direct DNA damage [5], intracellular optical breakdown and plasma formation [6], etc. The linear damage mechanism (heating), however, is deemed dominant for pigment-rich tissues, such as skin and the retina. In these tissues, strong one-photon absorption of the infrared (IR) radiation due to a high concentration of pigments may lead to a significant local temperature increase, cavitation, and morphological damage, as was reported for skin tissue by Masters *et al* [7]. More recently, Paoli *et al* emphasized that

only a small increase in laser power over the threshold causes severe damage to the stratum corneum; thus, the possibility of thermal mechanical damage must be safely controlled in order to bring MPM into clinical practice [8]. The first commercial MPM imaging system approved in Europe for *in vivo* diagnostics of human skin, *DermaInspect* [9], has therefore been equipped with Ti:sapphire laser oscillators featuring an output pulse width of ∼75 fs, which is a factor of two smaller than that of conventional MPM imaging systems.

The diversity of imaging conditions and concomitant requirements on the laser pulse duration, inferred from the discussion above, can feasibly be accessed using a single broadband laser source. The pulse shape and energy at the focal (imaging) plane should then be carefully controlled, and the combination of an ultrafast laser and a pulse shaper allows doing exactly that. Using the pulse shaper and one of available pulse measurement techniques, such as multiphoton intrapulse interference phase scan (MIIPS) [10–12], it is possible to correct for pulse distortions introduced by the dispersive optical elements of the microscope setup. With ultrashort transform-limited (TL) pulses to start with, one can use the same shaper to add a pre-programmed amount of dispersion and adjust the pulse duration over a large time range. The added phase distortion can be as simple as a linear chirp, but the same system can be used to implement more advanced pulse shaping schemes, e.g., selective two-photon excitation of fluorophores [13–15], or even other modalities of nonlinear microscopy such as second-harmonic generation (SHG) imaging and single-beam coherent anti-Stokes Raman scattering microscopy [16].

The actual types and mechanisms of damage that are inflicted by the laser pulse illumination are not only sample dependent but also problem specific. The laser-induced effects range from easily observable changes in photobleaching rates to subtle changes in transgenic sequences that then form DNA expressing mutated malignancies [17]. Here we limit the observables to simple optical indicators of damage—morphology and frame-to-frame changes (increase or decrease) of the average two-photon excited (TPE) signal over the time of exposure. We review guidelines towards mitigation of the linear and NL damage, focusing on the optimization of two-photon microscopy imaging, and then describe two experimental studies comparing two-photon imaging with TL and linearly chirped pulses. The first is autofluorescence/SHG imaging of a transparent section of human melanoma tissue, and the other is TPE autofluorescence imaging of blood samples. Both types of samples are expected to absorb IR laser light due to the presence of either melanin (melanoma biopsy sample) or hemoglobin (blood) [18] and, therefore, exhibit interplay between the linear and nonlinear damage mechanisms.

2. Mitigation of photodamage in two-photon microscopy

An intuitive perspective on the optimization of pulse duration for laser-safe two-photon microscopy imaging can be obtained from the well-known scaling of n-order signal intensity, $S^{(n)}$, with input pulse energy E_p and duration τ,

$$S^{(n)} \propto (E_\mathrm{p}/\tau)^n \tau = E_\mathrm{p}^n \tau^{-(n-1)}. \tag{1}$$

Since we want to evaluate the linear and NL contribution as a function of pulse duration for two-photon imaging, it is advantageous to rewrite equation (1) to include the TPE excitation efficiency explicitly, i.e., in the form:

$$S^{(n)} \propto [S^{(2)}]^{n/2} \tau^{-(n/2-1)}. \tag{2}$$

The dependence on the pulse energy is now hidden in $S^{(2)}$ and we assume that there is no deficit for the laser power that can be delivered to the imaging plane. Equation (2) shows unambiguously that if the dominant damage mechanism is nonlinear and its order is higher than two, it is advantageous for two-photon microscopy to use longer pulses of higher energy. On the contrary, a low tolerance to heat favors shorter pulse duration and lower energy per pulse. This is because

$$S^{(1)} \propto [S^{(2)}]^{1/2} \tau^{1/2}, \tag{3}$$

i.e., the linear contribution increases with pulse duration when the TPE is kept constant by adjusting the laser power.

The thresholds imposed by the two contributions, as well as by detector sensitivity, are presented schematically by the log–log plots of figure 1. In this representation, the area of acceptable imaging parameters (laser-safe region shaded in gray) is bounded by three straight crossing lines. One of them (red solid line with the slope of -1) is determined by the threshold for the linear damage, $S^{(1)}_\mathrm{max}$, and satisfies the relation

$$S^{(2)}_\mathrm{heat} \propto [S^{(1)}_\mathrm{max}]^2 \tau^{-1}. \tag{4}$$

The second line (blue solid line with slope of $1 - 2/n$, where $n = 2$ or 3) is set by the threshold for the nonlinear damage, $S^{(n)}_\mathrm{max}$, and is defined by

$$S^{(2)}_\mathrm{nl} \propto [S^{(n)}_\mathrm{max}]^{2/n} \tau^{1-2/n}. \tag{5}$$

The third line is determined by the sensitivity of the imaging system (purple dashed horizontal line), dependent on collection losses and detector efficiency. Note that tuning the laser pulse duration while keeping its energy constant corresponds to scanning along a straight line of slope -1, parallel to the line defined by the linear damage threshold. This is consistent with the fact that the TPE signal is inversely proportional to the pulse duration, as follows from equation (1) for $n = 2$. To keep the TPE signal constant, one would need to adjust both pulse energy and duration simultaneously.

When the NL damage is induced primarily by the TPE itself, the model gives only the upper limit on the pulse duration, imposed by the linear damage; see figure 1(a). The lower limit will be dictated by either the finite two-photon absorption bandwidth and/or the turn-on of higher-order contributions at shorter pulse durations, which are not accounted for in this simplified picture. When the dominant NL mechanism is of higher order to start with ($n > 2$), there is an optimal pulse duration for the TPE signal, $S^{(2)}$, that

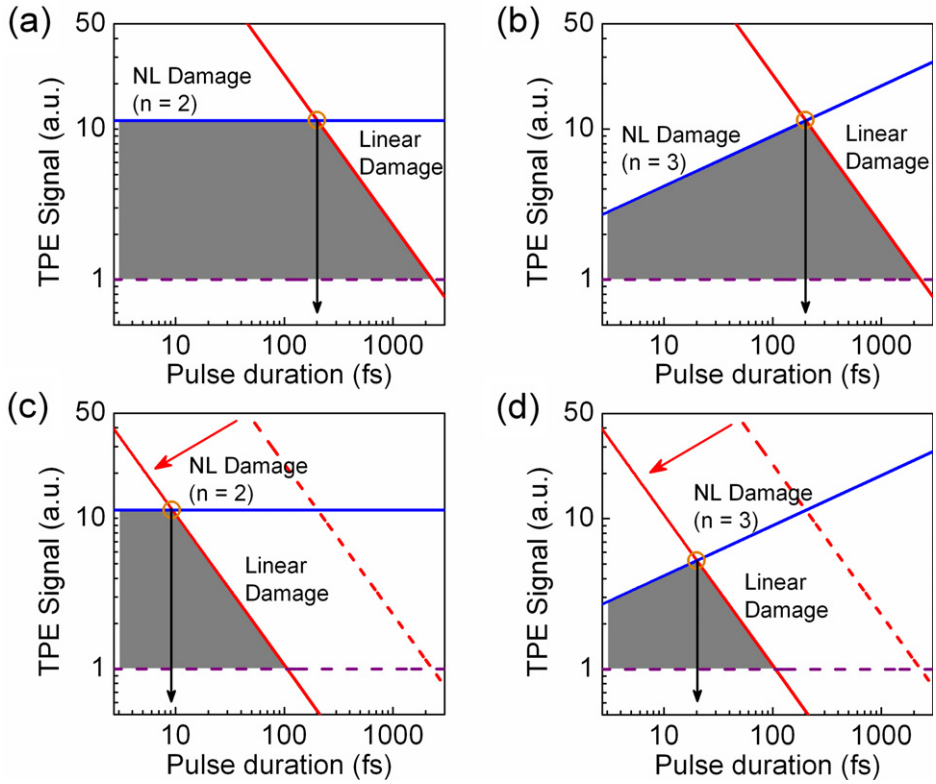

Figure 1. Optimization of laser pulse duration for two-photon microscopy imaging bounded by linear (heat) and NL photodamage. (a) Schematic presentation of laser-safe operational range for two-photon imaging of cellular structures and the majority of tissues. We assume here a second-order dependence of the NL damage threshold on laser power ($n = 2$) and use a common agreement that a pulse duration ∼150–200 fs is optimal in this case; (b) same as in (a) but assuming a third-order process ($n = 3$) as the dominant NL damage mechanism. ((c), (d)) Modified laser-safe operational range for two-photon imaging in the presence of increased linear absorption such as in melanin caps of human skin or hemoglobin-rich sections.

satisfies constraints (4) and (5); see figure 1(b). The actual value will vary from one case to another, dependent on the sample composition, but the general trends can be readily inferred from figure 1. For instance, if the optimal pulse duration for two-photon imaging of optically thin layers of cell cultures is about 200 fs, as in figure 1(b), the lower linear damage threshold for more absorbing tissues would shift the optimal pulse duration to lower values and, more importantly, might make the use of 200 fs pulses prohibitive for laser-safe imaging of those samples; see the illustration in figure 1(c) and (d). This observation can be another argument in favor of imaging systems that incorporate broadband laser sources and some means to control the pulse shape. They allow for straightforward pulse duration tuning over a large time span, with the lower limit inversely proportional to the spectral bandwidth of the laser.

Some important points that have been left out from the qualitative discussion above are: what to use as markers of photo-induced damage, how to quantify it and set a threshold. In the study that follows, we monitor the TPE signal bleaching rate as well as its redistribution over the imaged region. However, more sophisticated and biologically relevant means to assess phototoxicity in living tissue, such as fluorescence changes of various Ca_2^+-indicators [2], cell vitality by post-exposure incubation [3], and densitometric measurements [5], have been reported elsewhere.

3. Experimental details

Our experimental setup is almost identical to the one described in detail elsewhere [19]. Briefly, we utilize a Ti:sapphire laser oscillator (KMLabs, 86 MHz rep. rate) delivering IR light of ∼100 nm FWHM bandwidth centered at 810 nm. A prism-pair compressor and a folded-4f pulse shaper with a dual-mask one-dimensional 640 pixel spatial light modulator (CRi SLM-640-D-VN, Cambridge Research & Instrumentation, Inc.) are used to correct for pulse distortions and deliver pre-defined optical waveforms to the imaging plane.

We use the MIIPS technique to correct for pulse distortions. For that purpose, a thin KDP crystal, mounted on a microscope cover glass slide, is placed at the focus of the objective prior to the phototoxicity measurements. The spectrally resolved SHG signal from the nonlinear crystal, collected with a fiber-coupled USB4000 Ocean Optics spectrometer, is used as a feedback signal for MIIPS. The retrieved phase compensation mask is then added to all phase functions, programmed onto the SLM. The FWHM time duration of compressed pulses is about 13.6 fs.

The attenuated laser beam is raster scanned by a galvanic scanner (QuantumDrive-1500, Nutfield Technology, Inc.) and coupled into a water-immersion objective (Zeiss LD C-APOCHROMAT 40×/1.1, working distance of 0.62 for a 0.17 mm thick cover glass), mounted in an

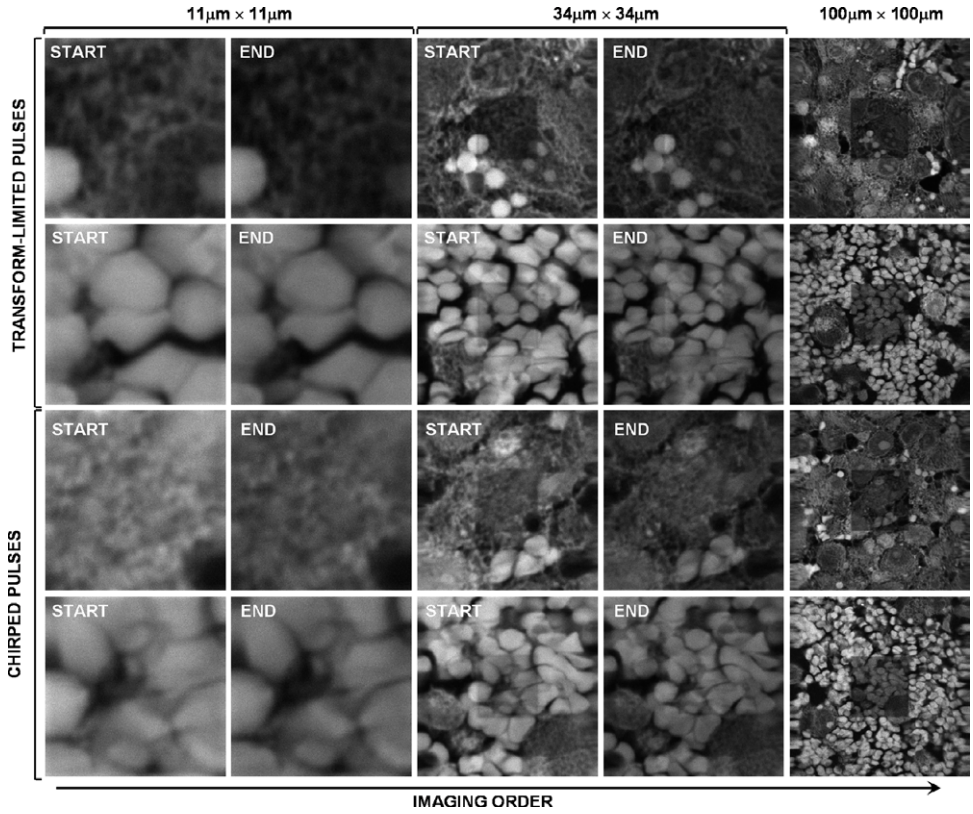

Figure 2. Representative imaging sequences of human melanoma tissue section obtained with TL and linearly chirped pulses. The sample is exposed to focused laser light, which is raster scanned consecutively over 11 μm × 11 μm and 34 μm × 34 μm areas (512 pixels × 512 pixels) at the speed of 1 frame s^{-1}. The exposure time is about 4 min. The 'start' and 'end' images are averaged over 20 frames, while the final 100 μm × 100 μm zoom-out image is averaged over 40 frames. The average laser power at the sample is about 2.1 mW for TL pulses and 7.2 mW (3.4 times higher) for chirped pulses.

adapted Nikon Eclipse TE-200 inverted microscope. The autofluorescence/SHG signal is separated from the scattered excitation light with a dichroic mirror (700DCSPXR, Chroma Technology Corp.) and then filtered further using a shortpass emission filter (ET680-SP-2P8, Chroma Technology Corp.). It is collected with a photomultiplier tube (PMT, HC120-05MOD, Hamamatsu) in the de-scanned mode.

We investigate two types of samples. One is a paraffin section (∼5 μm thick) of a human melanoma xenograft, obtained by sectioning a dense tumor volume of 50–60 mm originating from sub-cutaneous injection of SK-MEL-28 human melanoma cells into a nude mouse. The other is rabbit blood samples in two different forms: (i) dried drops of rabbit blood, with no prior preparation; (ii) red blood cells extracted from rabbit blood by fractionation. In the latter case whole blood is centrifuged at 500 × g at 25 °C for 10 min and the plasma is removed. The remaining red blood cells are then resuspended and washed three times in a phosphate buffered saline (PBS) solution. Next, a volume of 25 μl is pipetted on a slide and left to dry in a hood. Finally, the cells are fixed with paraformaldehyde (PFA) for 10 min, washed three times for 5 min with PBS, and glued with Biomeda gel mount.

To infer the effect of pulse shaping on the phototoxicity, the samples are imaged using TL pulses and linearly chirped pulses, having second-order dispersion of 1000 fs^2. The encoded 1000 fs^2 chirp stretches the originally 13.6 fs pulses to about 280 fs, i.e., by a factor of 20. The input laser power is tuned so that TPE efficiency remains constant. The proper power ratios are found experimentally by measuring the total SHG signal from the nonlinear crystal at the focus of the objective and adjusting the input power with variable neutral-density filters to match the integrated SHG photon counts for the two waveforms. The samples are exposed to the laser light of variable pulse shape and power under typical imaging conditions, when 512 pixel × 512 pixel images are recorded at a 1 frame s^{-1} rate. The average laser power at the melanoma sample is about 2.1 mW for TL pulses and 7.2 mW for chirped pulses. The size of imaged area varies as explained below. The TPE signal, averaged over the imaged section, is then plotted as a function of the total laser exposure time.

For the phototoxicity study of human melanoma tissue, a small 11 μm × 11 μm area of tissue is first exposed to the laser light. Next, we increase the imaging area to 34 μm × 34 μm about the damaged spot and repeat the measurement. At the end, we record an image of the exposed area, zooming out to 100 μm × 100 μm. In the analysis, we separate the data of the cytoplasmic portion of the malignant melanoma cells and red blood cells. The averaged signal from cytoplasm and red-blood-cell-rich areas exhibit a somewhat different dependence on the exposure time (frame number).

Because of the different character of the laser-induced damage in dried blood samples, the procedure is slightly

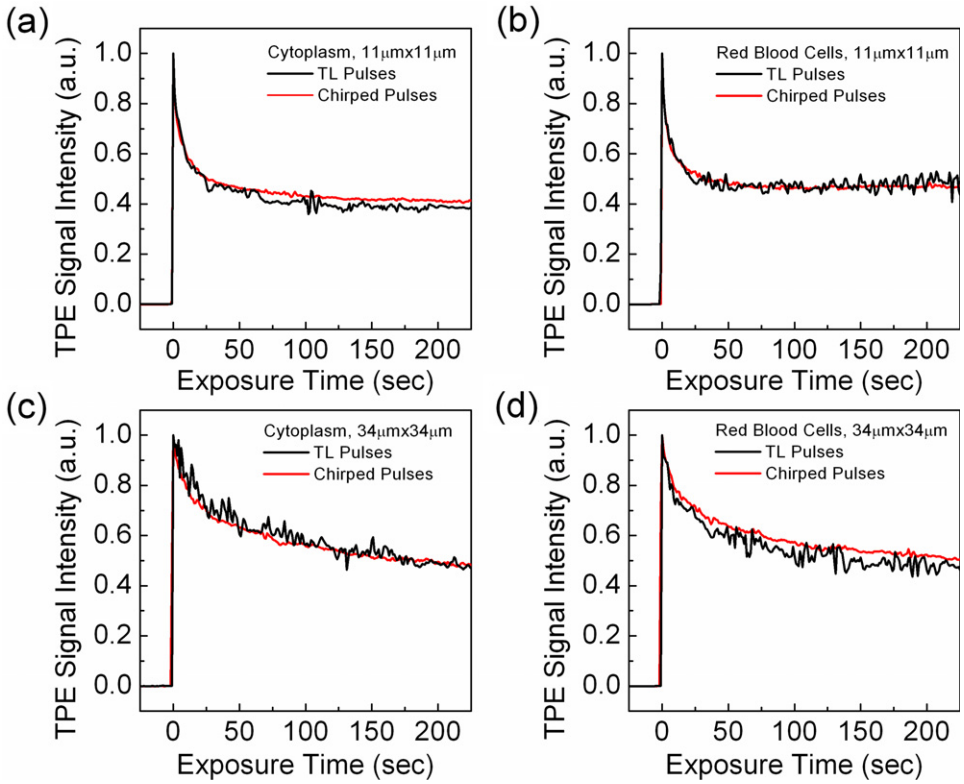

Figure 3. Normalized TPE signal intensity as a function of laser light exposure time (raster scan rate—1 frame s^{-1}) for TL and linearly chirped pulses. The amount of second-order dispersion is set to be 1000 fs^2. The exposed areas are: ((a), (b)) 11 μm × 11 μm or ((c), (d)) 34 μm × 34 μm, and feature: ((a), (c)) cytoplasm, ((b), (d)) red blood cells. The laser power is adjusted to maintain similar TPE efficiency for the two optical waveforms.

modified when imaging those samples. For every blood sample, we first record a 40-frame averaged zoom-out 150 μm × 150 μm image using low-energy TL pulses and then expose a 45 μm × 45 μm section at the center to shaped pulses of corresponding energy. Another 150 μm × 150 μm image using a low-power beam of TL pulses is recorded at the end. The input average power is 2.2 mW for TL pulses and 7.8 mW for chirped pulses except if indicated otherwise.

4. Results and discussion

Following the procedures outlined in section 3, we have collected data from human melanoma tissue and blood samples. Images from a typical data set for melanoma tissue are shown in figure 2. TPE signal dependencies for cytoplasm and red blood cells are summarized in figure 3.

As one can see, the prolonged exposure of a melanoma xenograft sample to raster scanned light leads to partial bleaching of the TPE signal. The bleaching rates are slightly different for cytoplasmic and red-blood-cell-rich areas and dependent on the laser dwell time as follows from data for 11 μm × 11 μm and 34 μm × 34 μm sections. However, we observe no appreciable dependence of the TPE signal photobleaching rates on the pulse shape for the two waveforms for the chosen pulse energies and exposure time. It suggests that in these experiments the dominant damage mechanism is two-photon in nature and, therefore, independent of pulse duration (for constant TPE) as long as heating is negligible. This hypothesis is also supported by the fact that the observed changes in brightness are confined to the raster scan region.

The photobleaching profiles in figure 3 are reproducible across the sample under the given imaging conditions. However, the photobleaching kinetics starts to vary significantly from one imaged area to another if one increases the average laser power at the sample or extends the exposure time (data not shown). In some cases we found that lowering the power level below the immediate bleaching threshold resulted in a localized onset of enhanced photo-emission that was usually followed by notable morphological changes—cell structure became more pronounced. While such events occur in both cytoplasm and red-blood-cell-rich areas, we have found them to be more prominent for red blood cells. An early pre-cursor of the photo-enhancement can be seen in figure 3(b) after about 100 raster scans (1 frame s^{-1}), where the average TPE signal starts to increase. The last observation justifies our transition to two-photon imaging of rabbit blood.

Representative images obtained from dried drops of rabbit blood are shown in figure 4. Note that for TL pulses there is little or no difference between the images taken before and after prolonged laser exposure. The effect on the average TPE signal across the image is minimal. The image sequences taken with chirped pulses, on the other hand, feature significant photobleaching and/or photo-enhanced autofluorescence emission. The last point is well

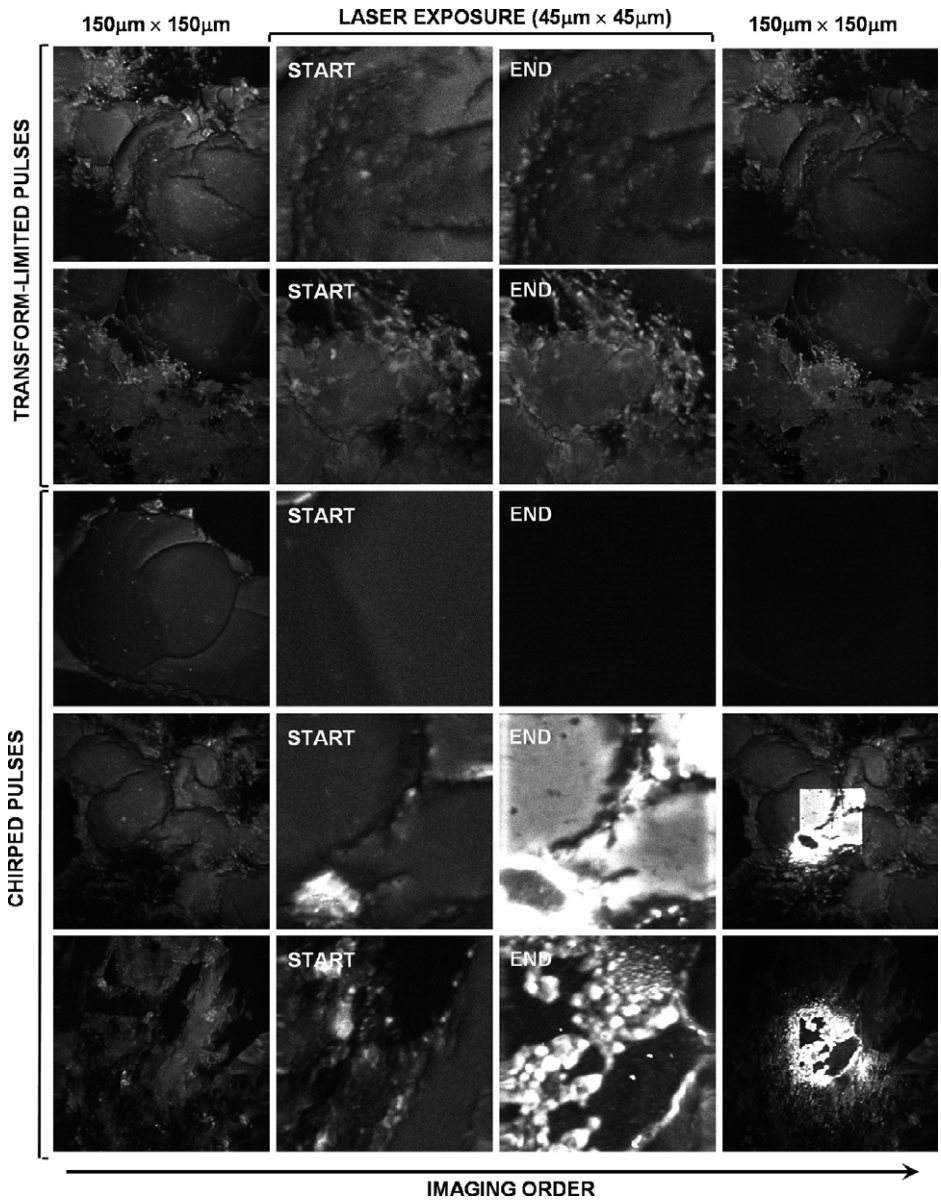

Figure 4. Representative imaging sequences recorded on dried blood samples using TL and linearly chirped pulses. The laser power is adjusted to maintain similar TPE efficiency. The 150 μm × 150 μm zoom-out images before and after prolonged laser light exposure are obtained using low-energy TL pulses, averaging over 40 frames. The 45 μm × 45 μm areas are raster scanned by the focused beam of shaped laser light at the speed 1 frame s^{-1} (512 pixels × 512 pixels). The exposure time is about 3 min. The 'start' and 'end' images are averaged over 20 frames.

illustrated by average TPE autofluorescence intensities plotted as a function of exposure time in figure 5. The average signal in some cases increases by as much as 30–40 times (out of the scale in figure 5). Morphological changes are profound, and are not limited to the exposed 45 μm × 45 μm area. The laser-induced damage is typically accompanied with the formation of 'hot' (bright) spots within and beyond the imaged area. The 'hot' spots eventually bleach out, and the average TPE signal decreases.

The measurements on fractionated fixed rabbit red blood cells reveal similar autofluorescence kinetics but at higher input laser energies. Illuminating the cells with 18 mW of average laser power (TL pulses) for 2 min causes a gradual 10-fold increase in fluorescence intensity; as shown in figures 6(a)–(c) and (e). This process is not preceded by photobleaching as in measurements on the melanoma sample in figure 2. However, the photobleaching becomes apparent at 3× lower laser power (6 mW), as illustrated in figure 6(e) on the 4 min long interval in between laser-off windows. When we switch back to 18 mW power, the fluorescence again exhibits photo-enhancement and rises by up to a 15-fold level by the end of the scan; see figures 6(d) and (e).

5. Conclusions

In this study, we have proposed a model for establishing the dominant contributions to laser-induced damage during

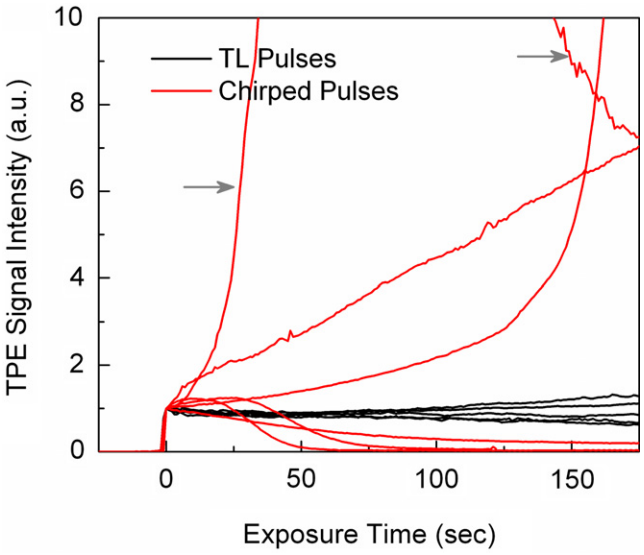

Figure 5. Normalized TPE signal intensity as a function of laser light exposure time (raster scan rate—1 frame s^{-1}) for TL and linearly chirped pulses. The laser power is adjusted to maintain similar TPE efficiency by the two optical waveforms. Gray arrows highlight the average TPE signal intensity for the case where the photo-enhancement factor reached a maximum value of 30.

MPM imaging. Experimentally, we evaluate the effect of pulse duration on laser-induced damage during two-photon autofluorescence imaging of unstained samples. In our experiments, the photodamage is evidenced by both photobleaching and photo-enhancement of autofluorescence. The earlier process exhibits identical bleaching rates for TL (∼14 fs) and chirped (∼280 fs) pulses, provided that the average laser power is adjusted to maintain similar starting TPE. Under the same conditions, the observed photo-enhancement of endogenous autofluorescence favors longer pulses.

Although our observations are preliminary, the enhanced autofluorescence spectrum, peaking at 460–470 nm, is consistent with that of NADH [20]. The possible mechanism for this enhancement is that electrons generated at the high laser intensity reduce NAD^+, converting it to NADH. One-photon absorption spectra of NAD^+ and NADH differ greatly in the 300–390 nm region, where NAD^+ has very limited absorbance [21]. The spectral shift of absorption associated with the reduction process would be consistent with greater two-photon absorption in the 800 nm region of the laser, and the observed enhanced fluorescence. Morphological changes begin to take place after the photo-enhancement.

As we extrapolate our results to other imaging situations, we have learned that ultrashort pulses provide an excellent nonlinear optical signal while depositing a minimal amount of heat. This property is of particular interest for applications *in vivo* such as in dermatology where the laser energy dissipates in the tissue and can cause thermal damage.

Acknowledgments

This work was partially funded by the National Science Foundation Chemical Research Instrumentation Funds—Instrument Development 0923957. We would like to thank Dr James Resau and Dr Nicholas Duesbery (Van Andel Research Institute, Grand Rapids, MI) for melanoma xenograft samples and Professor Dana Spence (Department of Chemistry, MSU, East Lansing, MI) for rabbit blood samples used in these experiments. We are grateful for funds recently available from NIH grant 1R21EB008843.

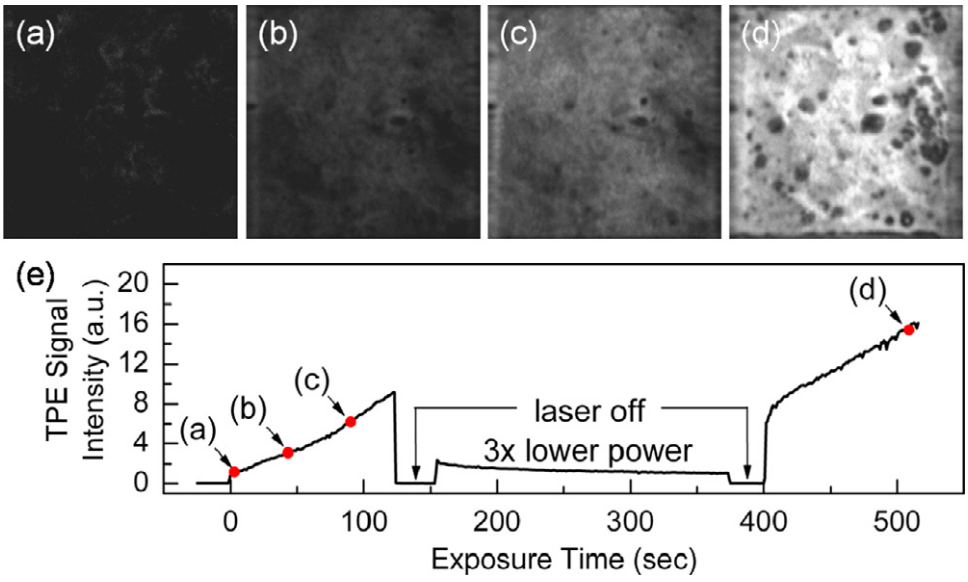

Figure 6. An example of photo-enhancement as visualized by two-photon microscopy imaging. Red blood cells are exposed to focused laser light, which is raster scanned over a 34 μm × 34 μm area (512 pixels × 512 pixels) at the speed of 1 frame s^{-1}. Snapshots ((a)–(c)) are taken 45 s apart (0, 45, 90) with the average of 25 consecutive frames. Image (d) is taken at the end of the scan. (e) Normalized TPE signal intensity as a function of laser light exposure time under variable conditions. The initial 18 mW laser light exposure is followed by laser-off, 3× lower power (240 s long, ∼6 mW), and further laser-off intervals. Further photo-enhancement of autofluorescence is observed when the starting illumination conditions are restored. The overall fluorescence increase is over 15-fold.

References

[1] Denk W, Strickler J H and Webb W W 1990 Two-photon laser scanning fluorescence microscopy *Science* **248** 73–6

[2] Koester H J, Baur D, Uhl R and Hell S W 1999 Ca2+ fluorescence imaging with pico- and femtosecond two-photon excitation: signal and photodamage *Biophys. J.* **77** 2226–36

[3] Konig K, Becker T W, Fischer P, Riemann I and Halbhuber K J 1999 Pulse-length dependence of cellular response to intense near-infrared laser pulses in multiphoton microscopes *Opt. Lett.* **24** 113–5

[4] Hopt A and Neher E 2001 Highly nonlinear photodamage in two-photon fluorescence microscopy *Biophys. J.* **80** 2029–36

[5] Shafirovich V, Dourandin A, Luneva N P, Singh C, Kirigin F and Geacintov N E 1999 Multiphoton near-infrared femtosecond laser pulse-induced DNA damage with and without the photosensitizer proflavine *Photochem. Photobiol.* **69** 265–74

[6] Konig K, Riemann I, Fischer P and Halbhuber K H 1999 Intracellular nanosurgery with near infrared femtosecond laser pulses *Cell. Mol. Biol.* **45** 195–201

[7] Masters B R, So P T and Gratton E 1997 Multiphoton excitation fluorescence microscopy and spectroscopy of *in vivo* human skin *Biophys. J.* **72** 2405–12

[8] Paoli J, Smedh M, Wennberg A-M and Ericson M B 2008 Multiphoton laser scanning microscopy on non-melanoma skin cancer: morphologic features for future non-invasive diagnostics *J. Invest. Dermatol.* **128** 1248–55

[9] Schenke-Layland K, Riemann I, Damour O, Stock U A and Konig K 2006 Two-photon microscopes and *in vivo* multiphoton tomographs—powerful diagnostic tools for tissue engineering and drug delivery *Adv. Drug Deliv. Rev.* **58** 878–96

[10] Lozovoy V V, Pastirk I and Dantus M 2004 Multiphoton intrapulse interference. IV. Ultrashort laser pulse spectral phase characterization and compensation *Opt. Lett.* **29** 775–7

[11] Xu B W, Gunn J M, Dela Cruz J M, Lozovoy V V and Dantus M 2006 Quantitative investigation of the multiphoton intrapulse interference phase scan method for simultaneous phase measurement and compensation of femtosecond laser pulses *J. Opt. Soc. Am.* B **23** 750–9

[12] Coello Y, Lozovoy V V, Gunaratne T C, Xu B W, Borukhovich I, Tseng C H, Weinacht T and Dantus M 2008 Interference without an interferometer: a different approach to measuring, compressing, and shaping ultrashort laser pulses *J.Opt. Soc. Am.* B **25** A140–50

[13] Pastirk I, Dela Cruz J M, Walowicz K A, Lozovoy V V and Dantus M 2003 Selective two-photon microscopy with shaped femtosecond pulses *Opt. Express* **11** 1695–701

[14] Ogilvie J P, Debarre D, Solinas X, Martin J L, Beaurepaire E and Joffre M 2006 Use of coherent control for selective two-photon fluorescence microscopy in live organisms *Opt. Express* **14** 759–66

[15] Isobe K, Suda A, Tanaka M, Kannari F, Kawano H, Mizuno H, Miyawaki A and Midorikawa K 2009 Multifarious control of two-photon excitation of multiple fluorophores achieved by phase modulation of ultra-broadband laser pulses *Opt. Express* **17** 13737–46

[16] Dudovich N, Oron D and Silberberg Y 2002 Single-pulse coherently controlled nonlinear Raman spectroscopy and microscopy *Nature* **418** 512–4

[17] Cruz J M D, McMullen J D, Williams R M and Zipfel W R 2010 Assessing the mutagenicity potential of multiphoton excitation during imaging of intrinsic fluorescence from cells and tissues *Biophys. J.* **98** 576a

[18] Schonle A and Hell S W 1998 Heating by absorption in the focus of an objective lens *Opt. Lett.* **23** 325–7

[19] Xi P, Andegeko Y, Pestov D, Lovozoy V V and Dantus M 2009 Two-photon imaging using adaptive phase compensated ultrashort laser pulses *J. Biomed. Opt.* **14** 014002

[20] Huang S H, Heikal A A and Webb W W 2002 Two-photon fluorescence spectroscopy and microscopy of NAD(P)H and flavoprotein *Biophys. J.* **82** 2811–25

[21] Mayevsky A and Rogatsky G G 2007 Mitochondrial function *in vivo* evaluated by NADH fluorescence: from animal models to human studies *Am. J. Physiol.-Cell Physiol.* **292** C615–40